IEEE Access
Multidisciplinary | Rapid Review | Open Access Journal

Received January 28, 2019, accepted February 18, 2019, date of publication February 26, 2019, date of current version March 8, 2019.

Digital Object Identifier 10.1109/ACCESS.2019.2900958

New Modified Urban Canyon Models for Satellite Signal Propagation Prediction

HOSSEIN HADIDIAN MOGHADAM, (Member, IEEE), AND AMMAR B. KOUKI, (Senior Member, IEEE)
Electrical Department, École de technologie supérieure, Montreal, QC H3C 1K3, Canada

Corresponding author: Hossein Hadidian Moghadam (hossein.hadidianmoghadam.1@ens.etsmtl.ca)

ABSTRACT The effects of high-rise buildings on satellite propagation in the vicinity of urban canyons are investigated. A comparison between a conventional canyon model and the two modified canyon models, which take into account the presence of high-rise buildings, is presented for both narrow-band and wideband signal cases. The narrow band is developed using ray tracing (RT) and includes the direct wave, the specular reflection from building walls and ground, and the diffracted waves. In addition, multiple shadow boundaries are defined and used to carry out the uniform theory of diffraction calculations. The incident shadow boundary is the dominant boundary and is used to determine the line-of-sight region for all cases, while wall and ground reflection shadow boundaries are used to obtain higher precision due to multiple reflections. The wideband model is developed by applying a channel transfer function to the data obtained from the RT method. The proposed models are used to predict the received signal in a realistic urban environment from satellites. The models are applicable to any satellite link application, such as global navigation satellite systems, low Earth-orbiting, and high-altitude platform systems, and the results are obtained for a satellite transmitting two linearly polarized signals at a frequency of 1.625 GHz. It is found that the presence of high-rise buildings next to a street canyon can significantly alter the visibility of satellites, which, in turn, lead to an increase in path loss. Consequently, ignoring high-rise buildings in the proximity of a street canyon can lead to a path loss difference of as much as 30 dB.

INDEX TERMS Street canyon, conventional canyon model (CCM), non-line of sight (NLOS), ray tracing (RT), uniform theory of diffraction (UTD).

I. INTRODUCTION

Satellite and high altitude platform systems (HAPS) are large coverage-area non-terrestrial radio systems that have many applications, such as wireless communication, navigation and remote sensing with varying bandwidth requirements. Having an accurate signal propagation model, especially in urban environments, is vital for link budget analysis, system's margins determination, dimensioning, and prediction of coverage and outage areas, as well as for the development of techniques to overcome related problems. This is particularly important in areas with high-rise buildings because they cause shadowing, leading to spotty coverage for HAPS [2]–[9]. In developing accurate propagation models, two issues need to be addressed mainly: (i) the bandwidth of the model, i.e., narrow-band vs. wide-band, and (ii) its nature, i.e., deterministic vs. statistical (random).

Early studies on wide-band propagation techniques based on the uniform theory of diffraction (UTD) were proposed in [10] and [11]. However, those are limited to terrestrial radio systems. In Tirkas *et al.* [12], using ray tracing (RT), a narrow-band deterministic LEO satellite signal propagation model was introduced with just one single building in a flat terrain. Deterministic propagation models for LEO satellites, including narrow-band and wide-band simulation, were proposed by Blazevic *et al.* [13]. In these models, the urban and suburban environments were considered to be of the street canyon type. Using UTD and RT, the path loss curves in a narrow-band around a carrier frequency of 1.625 GHz were calculated [13]. Additionally, the wide-band path loss was also derived from the channel transfer function [13]. In [14], Meedović and Šuka presented a survey of several propagation software packages, which included physical-based

The associate editor coordinating the review of this manuscript and approving it for publication was Vittorio Degli-Esposti.

statistical methods, such as Okumura-Hata, OPAR, Triple Path Geodesic and Walfish-Ikegami, in addition to a deterministic RT method for terrestrial propagation in urban environments using a canyon model.

Iglesias and Sánchez [15] and Lemos Cid *et al.* [16] presented a statistical wide-band analysis for low-elevation satellites based on measured data for channel characterization considering urban, suburban, rural, lightly wooded and heavily wooded environments. In [17]–[19], a narrow-band technique was applied for detecting the Global Navigation Satellite System (GNSS) availability in different geographical areas. Moreover, in [1], a method for optimizing the accuracy of GNSS receivers in urban environments in particular was developed by modeling signals with pseudorange error only. The geometrical model used for the urban environments in the aforementioned references ([1], [17]–[19]) was the conventional street canyon model.

Zeleny *et al.* [20] presented a semi-deterministic model combining 2D RT and stochastic methods. The canyon model was applied to built-up areas. Li *et al.* [21] and Jost *et al.* [22] presented a hybrid model for satellite propagation, including deterministic and statistical approaches. They applied narrow-band and wide-band simulation techniques, respectively. In [23]–[26], physical-statistical models, composed of specular reflection and incoherent scattering techniques, are presented. The electric field integral equations were solved by using the method of moments.

The conventional urban canyon model has been used in almost all 2D propagation simulations in urban environments. However, such a model can be overly simplistic in certain urban areas with multiple high-rise buildings by neglecting key ray contributions. To overcome this limitation, two new models, referred to as modified canyon models (MCMs), are proposed in this paper. The deterministic coverage prediction of a low-earth orbiting (LEO) satellite signal in urban environments is presented for the conventional and modified canyon models. The propagation path loss is computed by applying 2D RT and UTD, including single and double edge diffraction. In addition, both narrow-band and wide-band path loss modeling are addressed to cover different applications with varying bandwidth requirements. The remainder of the paper is organized as follows: section II introduces the modified canyon models and presents the narrow-band and wide-band propagation models for all of them. Section III presents the simulation results for the proposed models and compares them to the conventional canyon model. Finally, conclusions and perspectives are presented.

II. PROPAGATION MODELING FOR CANYONS AND MODIFIED CANYONS

A. PROPAGATION PATH LOSS

Signal propagation between a satellite and a receiver located in an urban environment can be split into two main components: (i) a line of sight [1] component and (ii) a multipath component due to the presence of buildings around the receiver. The total path loss in dB can then be written as:

$$L_t = L_o + L_{urban} \tag{1}$$

where L_o denotes the free space path loss corresponding to the LOS component and computed by the Friis' formula [10] and L_{urban} is the loss due to reflection and diffraction from buildings and ground corresponding to the multipath component and computed by RT, including UTD.

B. GEOMETRICAL MODEL CONSTRUCTION

For this study, we consider the urban environment of downtown Montreal, Canada, as shown in Fig. 1. This is a typical urban environment with street canyons and various high-rise buildings.

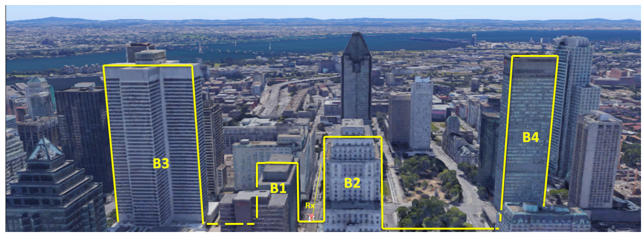

FIGURE 1. A sample illustration of blockage by high-rise buildings in the city center of Montreal.

If a LEO satellite is positioned over the city at elevation θ_o, and a satellite receiver is located in a street canyon, then the vertical plane containing the line that connects the satellite and the receiver can be used as the geometry plane of the model. Using this construct, one can extract the simplified geometrical models shown in (Fig. 2). This simplification, allows us to capture the main propagation contributions without having to carry out more costly, albeit more accurate, 3D ray tracing simulations as in [27] and [28] where commercial tools were used. Fig. 2a represents the conventional canyon model CCM, which considers only two buildings, B_1 and B_2, neighboring the receiver. Fig. 2b presents the first modified canyon model, MCM1, which includes one additional tall building on either side of the conventional street canyon. Fig. 2c shows the second modified canyon model, MCM2, which includes two additional tall buildings, B_3 and B_4, on either side of the conventional canyon model.

C. PROPAGATION MODEL VIA RAY TRACING (NARROW-BAND)

In order to predict the satellite signal in urban environments, a deterministic method in the form of RT combined with UTD is applied. The basic idea of this method is to introduce electromagnetic waves represented as rays that travel from the satellite to the receiver, located between B_1 and B_2, and which are subject to specular reflection from the ground and building walls and diffraction at building edges. For a complete understanding of the propagation model, the propagation environment must be fully described. A single building urban propagation model has been reported in [12].

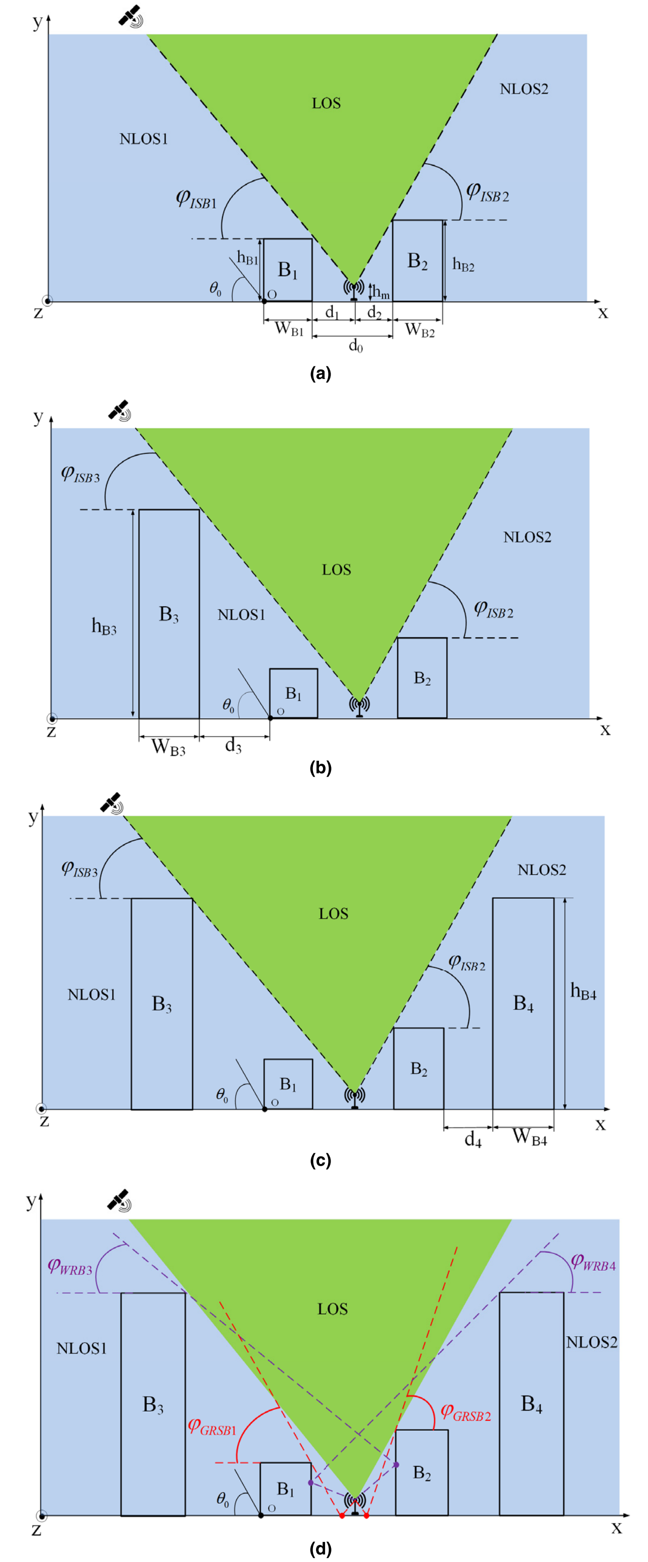

FIGURE 2. Geometry of (a) CCM. (b) MCM1. (c) MCM2 and (d) MCM2 with shadow boundaries.

This model is not suitable for a case like an urban canyon with multiple buildings, since it ignores reflections and blockages that can occur due to the presence of additional buildings.

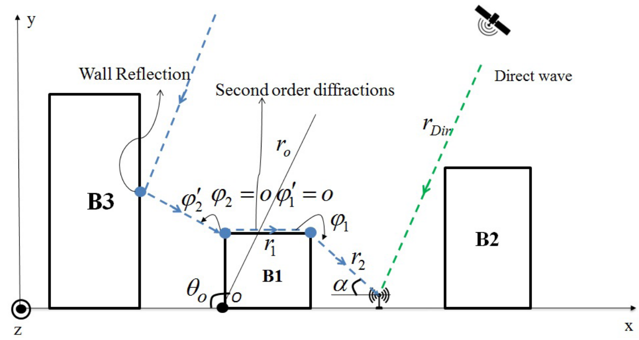

FIGURE 3. Direct wave and wall reflection from building B_3 and second order diffraction from building B_1.

It may however be suitable for suburban areas. In complex urban environments, such as the one illustrated in Fig. 1, the conventional canyon model (CCM) [13], [29]–[31] with two buildings only (B_1 and B_2), as shown in Fig. 2a, does not accurately predict the signal propagation because it does not take into account the presence of additional taller buildings. Indeed, as Figs. 2b and 2c show, the impact of the tall buildings (B_3 and B_4) may be quite significant in terms of line of sight region size, first and second order wall reflections, first and second order diffractions and possible blocking effects that occur at some satellite elevation angles.

In the 2D RT implementation all buildings are considered to be of infinite dimension in the z-direction perpendicular to the vertical plane, the satellite system is LEO and an elevation angle variation in the range of 0-180 degrees on the incident plane. The total received electric ($\vec{E}^r$) and magnetic ($\vec{H}^r$) fields at the receiver are the sum of N ray contributions and can be written as:

$$\begin{cases} \vec{E}^r = \sum_{n=1}^{N} \vec{E}_n \\ \vec{H}^r = \sum_{n=1}^{N} \vec{H}_n \end{cases} \tag{2}$$

The contributions ($\vec{E}_n, \vec{H}_n$) originate from the direct wave [1], ground reflections, first and second order building wall reflections, first and second order diffractions and other combinations of ground and wall reflections. Using this criterion, the number of ray contributions, including the direct ray, is found to be 26 for CCM, 62 for MCM1 and 73 for MCM2. It should be noted that diffuse scattering, due to surface roughness, and all higher order reflections and diffractions are neglected.

In general, the polarization of the incident wave from the satellite can be linear or circular, with linear polarization being either horizontal or vertical. Since a circular polarization can be decomposed into a sum of two linear polarizations, namely horizontal and vertical, circular polarization results can be obtained by linear superposition of those of the two linear polarizations.

$$\begin{cases} \vec{E}^r = \hat{z}E_z^r = \hat{z}\sum_{n=1}^{N} E_{zn}^r & \text{for horizontal polarization} \\ \vec{H}^r = \hat{z}H_z^r = \hat{z}\sum_{n=1}^{N} H_{zn}^r & \text{for vertical polarization} \end{cases} \tag{3}$$

For the sake of clarity and space, the propagation model will be derived for vertical polarization, i.e., using $\left(\vec{H}_r = \hat{z}H_{zr}\right)$. For horizontal polarization a similar approach can be followed by using the electric field instead, i.e., $\left(\vec{E}_r = \hat{z}E_{zr}\right)$.

For the i^{th} ray contribution the received magnetic field can be written as:

$$H_z^i(\omega) = \left|H_z^i(\omega)\right| e^{j\varphi_i(\omega)} \tag{4}$$

Assuming that the propagation channel varies slowly around the carrier frequency f_c with constant amplitude and linear phase such that a Taylor series expansion can be used:

$$\begin{cases} \left|H_z^i(\omega)\right| = \left|H_z^{ic}\right| \\ \varphi_{i(\omega)=}\varphi_{ic} + (\omega-\omega_c)\,\tau_i; \text{ where } \tau_i = \dfrac{d\varphi_i}{d\omega}\Big|_{\omega=\omega_c} \end{cases} \tag{5}$$

where φ_{ic} is the phase of $H_z^i(\omega)$ at ω_c and τ_i is the time delay of propagation along the i^{th} ray with respect to the direct ray contribution. Therefore, equation (4) can be rewritten as:

$$H_z^i(\omega) = \left|H_z^{ic}\right| e^{j\varphi_{ic}} e^{j\tau_i(\omega-\omega_c)} \tag{6}$$

The magnitude term, $\left|H_z^{ic}\right|$, depends on the geometry of the urban area (ground and building-wall reflections and edge diffractions), as well as on the receiving antenna gain pattern. Based on the procedure presented in [32], the magnitude of the baseband impulse response for the i^{th} ray contribution can be written as:

$$\left|r_z^i(t)\right| = 2\left|H_z^{ic}\right| \delta(t-\tau_i) \tag{7}$$

Equations (4) and (7) correspond to a single ray contribution. For multiple rays [32], the total magnetic field H_z^T, is given by:

$$H_z^T(\omega) = \sum_i H_z^i(\omega) = \sum_i \left|H_z^{ic}\right| e^{j\varphi_{ic}} e^{j\tau_i(\omega-\omega_c)} \tag{8}$$

with the channel's impulse response, given by:

$$\left|r_z^T(t)\right| = 2\sum_i \left|H_z^{ic}\right| \delta(t-\tau_i) \tag{9}$$

The impulse response and its corresponding frequency domain transfer function can be calculated for different elevation angles and different geometrical models, using the above described narrow-band propagation approach with RT and UTD. In each case, the rays are phase coherent and the number of the ray contributions depend on the satellite and the receiver positions and the geometrical models.

D. WIDE-BAND PATH LOSS

For non-geostationary satellites, the channel characteristics will be time varying. For linear time invariant systems, the impulse, i.e., the narrow-band model is sufficient. However in this case, with a linear time varying system, we must resort to building a wide-band channel model. Considering a stationary receiver, the wide-band path loss L_{WB} can be calculated following [13] as follows:

$$L_{WB}(f_k) = 10\log \frac{\int_{-\infty}^{\infty} X^2(f;f_k)df}{\int_{-\infty}^{\infty} \left|X(f;f_k).R(f)\right|^2 df} \tag{10}$$

where f is the radio frequency of the baseband, f_k the clock frequency, $R(f)$ is the complex function obtained by using the Fourier transform of the channel impulse response given in (7), and X the truncated frequency spectrum of a periodically repeated pseudo-noise (PN) waveform, which is given by:

$$X(f;f_k) = \begin{cases} \dfrac{\sin^2\left(\pi\frac{f}{f_k}\right)}{\left(\pi\frac{f}{f_k}\right)^2}, & |f| \le f_k \\ 0, & otherwise \end{cases} \tag{11}$$

E. CALCULATION OF BASEBAND IMPULSE RESPONSE FOR A RAY CONTRIBUTION

In order to compute the received satellite signal using RT and UTD, defining the shadow boundaries is a necessary first step [12]. The angle of each shadow boundary is calculated from the geometrical parameters of the specific canyon model being considered. Three shadow boundaries, namely the incident, ground reflection, and building wall reflection boundaries, are needed to analyze the LOS and NLOS ray contributions for the different propagation models. The LOS and NLOS regions for each model are highlighted in the corresponding figure in Fig. 2. The incident shadow boundaries for the CCM, i.e., φ_{ISB1} and φ_{ISB2}, are shown in Fig. 2a. For MCM1 and MCM2, the presence of building three, B_3, introduce a new incident shadow boundary, i.e., φ_{ISB3}, shown in Figs. 2b and 2c. Fig. 2d shows the ground reflection shadow boundaries due to buildings B_1 and B_2, φ_{GRSB1} and φ_{GRSB2}, respectively, as well as the wall reflection shadow boundaries due to buildings B_3 and B_4, φ_{WRSB3} and φ_{WRSB4}, respectively. Other shadow boundaries are always associated with the building that generates them and can be defined in similar manners taking into account the actual geometry of the model and the heights of the different buildings.

In Fig. 2b, extraction of the LOS and NLOS regions in MCM1, needs to consider the tall building B_3 in the MCM1 as a noticeable point. Hence, the LOS region will be between the maximum angle of two [φ_{ISB1}& φ_{ISB3}] and φ_{ISB2} (See Table 1). LOS and NLOS regions for MCM2 are presented in Table 1. Regarding the number of ray contributions, Table 1 represented a total review the number of ray

TABLE 1. **LOS and NLOS regions of propagation models in addition to number of ray contributions.**

	NLOS1		LOS		NLOS2	
	Angle Range	Rays	Angle Range	Rays	Angle Range	Rays
CCM	$0 \le \theta_o \le \phi_{ISB1}$	11	$\phi_{ISB1} \le \theta_o \le \pi - \phi_{ISB2}$	25	$\pi - \phi_{ISB2} \le \theta_o \le \pi$	11
MCM1	$0 \le \theta_o \le \max\begin{pmatrix}\phi_{ISB1} \\ \phi_{ISB3}\end{pmatrix}$	19	$\max\begin{pmatrix}\phi_{ISB1} \\ \phi_{ISB3}\end{pmatrix} \le \theta_o \le \pi - \phi_{ISB2}$	52	$\pi - \phi_{ISB2} \le \theta_o \le \pi$	15
MCM2	$0 \le \theta_o \le \max\begin{pmatrix}\phi_{ISB1} \\ \phi_{ISB3}\end{pmatrix}$	25	$\max\begin{pmatrix}\phi_{ISB1} \\ \phi_{ISB3}\end{pmatrix} \le \theta_o \le \max\begin{pmatrix}\pi - \phi_{ISB2} \\ \pi - \phi_{ISB4}\end{pmatrix}$	58	$\max\begin{pmatrix}\pi - \phi_{ISB2} \\ \pi - \phi_{ISB4}\end{pmatrix} \le \theta_o \le \pi$	25

contributions of the LOS and NLOS regions for the CCM and MCMs. As it mentioned before, the total number of ray contributions in CCM is 26. Since there are several common ray contributions in both LOS and NLOS regions, the number of ray contributions presented in Table 1 are 25 and 11 in LOS and NLOS regions, respectively. For the MCM1 and MCM2 the same reason is valid.

Considering MCM1 of Fig. 2b, there are 52 ray contributions in the LOS region as presented in Table 1. Here we will consider only two of these contributions to illustrate the equations that go into building the propagation model. One contribution is due to the wave reaching the receiver while the second includes wall reflection from building B_3 and second order diffraction from building B_1 shown in Fig. 3.

The normalized magnetic fields of direct H_z^{Dir} and wall reflected and second order diffracted field H_z^{WRD} with respect to the incident field at the reference point O are:

$$\begin{cases} H_z^{Dir}(\omega) = e^{-j\tau_1(\omega-\omega_c)} \\ H_z^{WRD}(\omega) = \Gamma_W(\psi).D^h\left(L_1, \varphi_1, \varphi_1^{'}, n_1\right) \\ D^h\left(L_{21}, \varphi_2, \varphi_2^{'}, n_2\right) \dfrac{e^{-j\tau_2(\omega-\omega_c)}}{\sqrt{r_1}\sqrt{r_2}} \end{cases}. \quad (12)$$

where $D^h\left(L, \varphi, \varphi', n\right)$ is the UTD building edge diffraction coefficient for vertical polarization [33] form of a lossy diffraction coefficient has been derived in [34] and Γ_W is the reflection coefficient [13]. The parameters τ_1 and τ_2 are the time delays of the direct and the building wall reflected-diffracted rays. Furthermore, the r_1 is distance between the two diffraction points on B_1 and r_2 is the distance between the second diffraction point and the receiver, as shown in Fig. 3. The angles of φ_1, φ_1', φ_2, φ_2' are indicated in the Fig. 3 and also n_1 and n_2 is the wedge index of first and second diffraction edges of B_1 [33].

The building permittivity ε_r is set to 5 for the selected frequency [13]. In (12) ωc is the carrier frequency as mentioned before assuming that the propagation channel varies slowly around that with constant amplitude and linear phase such that a Taylor series expansion is used [35].

The amplitude of transfer function is given by:

$$\begin{cases} \left|H_z^{Dir}(\omega)\right| = 1 \\ \left|H_z^{WRD}(\omega)\right| = \left| \begin{array}{l} \Gamma_W(\psi).D^h\left(L_1, \varphi_1, \varphi_1^{'}, n_1\right). \\ D^h\left(L_{21}, \varphi_2, \varphi_2^{'}, n_2\right). \dfrac{1}{\sqrt{r_1}\sqrt{r_2}} \end{array} \right| \end{cases} \quad (13)$$

Using (13) the narrow-band path loss can be calculated as:

$$L_{NB} = 20\log\left(\left|H_z(\omega)\right|\right) \quad (14)$$

Thus, the modulus of the baseband impulse response of this ray contribution is:

$$\begin{cases} \left|r_z^{Dir}(t)\right| = \delta(t-\tau_1) \\ \left|r_z^{WRD}(t)\right| = \left| \begin{array}{l} \Gamma_W(\psi).D^h\left(L_1, \varphi_1, \varphi_1^{'}, n_1\right). \\ D^h\left(L_{21}, \varphi_2, \varphi_2^{'}, n_2\right). \dfrac{1}{\sqrt{r_1}\sqrt{r_2}} \end{array} \right| \delta(t-\tau_2) \end{cases} \quad (15)$$

where the various geometrical parameters, r_1, r_2, φ_1, φ_2, $\varphi_1^{'}$, $\varphi_2^{'}$, L_{21}, L_1, n_1 and n_2 are:

$r_1 = W_{B1}$, $r_2 = d_1/\cos\alpha$, $\varphi_1 = o$, $\varphi_2 = \pi + \alpha$, $\varphi_1^{'} = \theta$, $\varphi_2^{'} = o$, $L_{21} = W_{B_1}$, $L_1 = \frac{r_1.r_2}{r_1+r_2}$, $n_1 = n_2 = 1.5$ and $\alpha = \tan^{-1}(\frac{h_{B_1}-h_m}{d_1})$.

A similar procedure is followed for all the rays in the canyon model being considered.

III. SIMULATION RESULTS AND COMPARISONS

For all simulations in this section, we assume a LEO satellite with carrier frequency fc = 1625 MHz, orbital altitude of 720 km and standard atmospheric propagation properties with the earth's radius of $r = 6366$ km. The complex permittivity for the ground and the buildings are given by $\varepsilon_r = 15\text{-}j90/f$ (f is the frequency in megahertz) and $\varepsilon_r = 5$, respectively [13]. Wide-band simulations are carried out with a channel bandwidth of 250 MHz, clock frequency $f_k = 125$ MHz and a maximal PN sequence of N = 2048. The electromagnetic wave at the receiver is normalized to the wave at the reference point (point o in Fig. 2).

First, we validate our method by considering the same scenario as the one presented in [12], which is a one building model. We use $h_B = 7$m and $w_B = 10$m for the height and width of the building, respectively, and a receiver – building distance of $d = 10$ m. The normalized signal level versus the satellite elevation angle is computed for horizontal and vertical polarizations and are shown in Figs. 4 and 5. These results are virtually identical to those in [12, Figs. 5 and 6]. As been seen the presence of a single building can generate as much as 40 dB variation in the received signal level, which for some applications such as GNSS may lead to a loss of position.

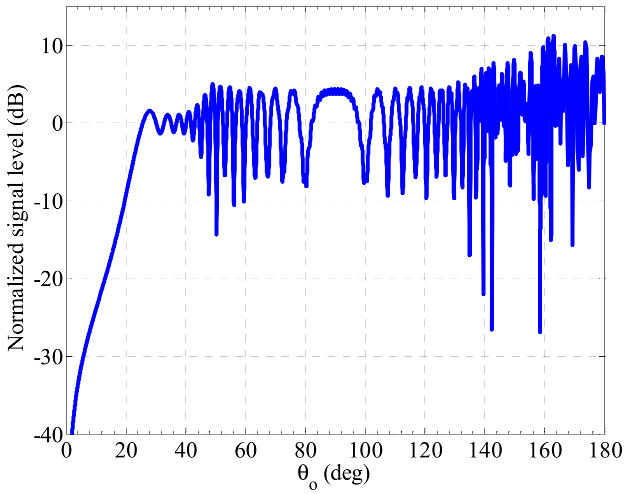

FIGURE 4. Normalized signal level versus satellite elevation angle for narrow-band simulation and horizontal polarization.

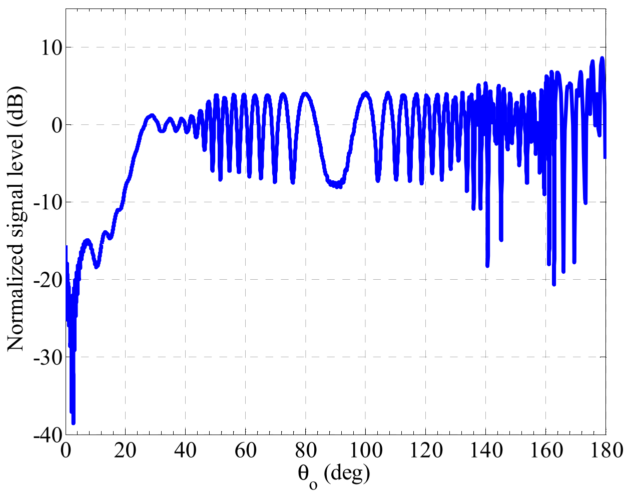

FIGURE 5. Normalized signal level versus satellite elevation angle for narrow-band and vertical polarization.

Next, we assess the impact of the presence of additional buildings on the conventional canyon model through two modified models. We start by carrying a comparative geometrical analysis of all models.

A. COMPARATIVE GEOMETRICAL ANALYSIS OF THE CC AND MC MODELS

In this section, we study in more detail the geometries of the CCM, MCM1 and the MCM2 to highlight the impact of the addition of tall buildings as well as the geometry of the buildings on the various shadow boundaries. To this end, we consider the building dimensions given in Table 2. These dimensions represent two tall 60 story buildings (B_3 and B_4) and two medium 13 story buildings between them (B_1 and B_2). These values are for Montreal's city center and are typical of urban environments. Based on these dimensions and using the equations in Table 1, we can see in Fig. 6 the variation of ISB angles due to the buildings in the geometrical models when the receiver moves from B_1 to B_2. The green and blue areas represent the LOS and NLOSs regions, respectively. Fig. 6a shows the variation of φ_{ISB1} and φ_{ISB2} in CCM versus the distance from building B_1 which is normalized to the corresponding street width (d_1/d_o). Fig. 6b demonstrates the φ_{ISB} angles due to three buildings B_1, B_2 and B_3. As it shows in this figure, the LOS region of the MCM1 compare to CCM reduces due to presence of B_3 when $d_1/d_o > 0.47$. Fig. 6c shows the φ_{ISB} angles in MCM2. The φ_{ISB3} is the same as MCM1 but B_4confines the LOS region up to $d_1/d_o = 0.52$.

TABLE 2. Geometrical parameters of CCM and MSMs.

Propagation Model	Dimensions (m)
CCM	d_o=30, d_1=15, d_2=15, w_{B1}=20, w_{B2}=20, h_{B1}=40, h_{B2}=40
MCM1	d_3=35, w_{B3}=50, h_{B3}=180
MCM2	d_4=35, w_{B4}=50, h_{B4}=180

B. PATH LOSS AND SIGNAL LEVEL CALCULATIONS FOR THE CCM AND THE MCMS

Using (10) and (14) and the model parameters of Table 2 the path loss level for the CCM and MCMs propagation models is calculated. Figs. 7 to 9 show the path loss versus the d_1/d_o for CCM, MCM1 and MCM2 at satellite elevation angles of $\theta_o = 30^\circ$ (Fig. 7), $\theta_o = 60^\circ$ (Fig. 8), and $\theta_o = 120^\circ$ (Fig. 9). As it mentioned before in this work the simulations include wide-band and narrow-band but to simplify graphs, only at $\theta_o = 30^\circ$ both propagation models are presented and in the remainder of graphs only wide-band simulation is used. As it shows in Fig. 6a, there is a rapid variation of the narrow-band path loss due to a number of ray contributions. Using (10) and (11), calculation of the wide-band path loss needs to integration of complex transfer function and the truncated frequency spectrum of a periodically repeated pseudo-noise (PN) waveform. Therefore as it shows in Fig. 6b the wide-band path loss has no more fluctuations. Regarding the path loss level at $\theta_o = 30^\circ$, as it shows in Figs. 6a, 6b and 6c receiver is NLOS1 area in all models. However, there is minimum 10 dB path loss difference between CCM and MCMs as it demonstrates in Fig. 7b. The difference corresponds to ray contributions mentioned in Table 1, such as double order diffractions/reflections from buildings B_3 and B_4. In $d_1/d_o < 0.56$ the ray contributions include first and second order diffractions from B_4 and reflections from B_1 leads to path loss reduction in MCM2.

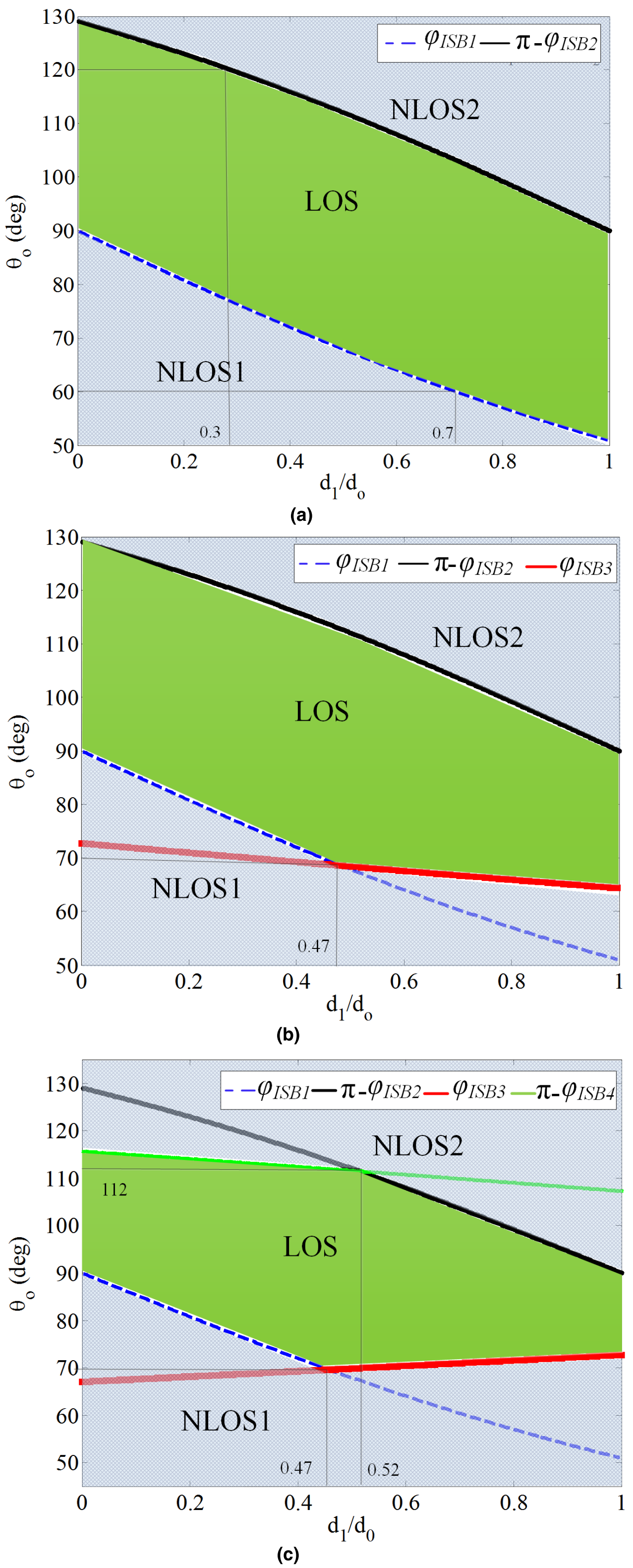

FIGURE 6. Variation of φ_{ISB} vs d_1/d_o in different propagation models. (a) CCM. (b) MCM1 and (c) MCM2.

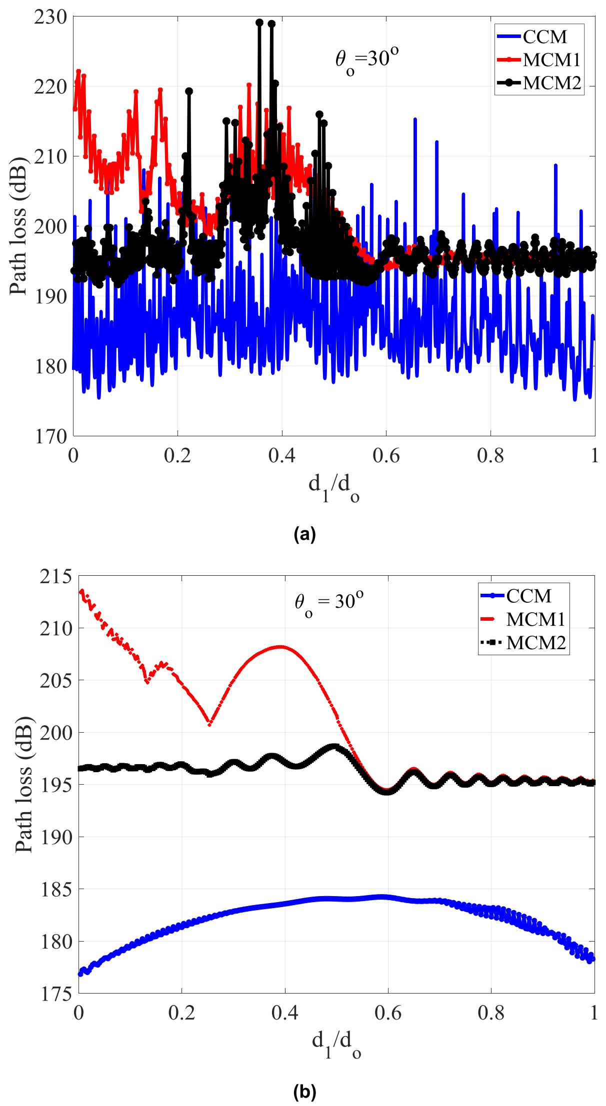

FIGURE 7. Comparison of path loss vs. d_1/d_o between CCM, MCM1 and MCM2 at $\theta_0 = 30°$ in vertical polarization. (a) Narrow-band path loss. (b) wide-band path loss.

At $\theta_o = 60^{\circ}$ MCM1 and MCM2 have approximately the same path loss level when the receiver moves from B_1 to B_2 as shown in Fig. 8. The fact that these results are so close is due to the dominant ray contributions at this elevation angle being made of the first order diffractions and the combination of the diffractions and wall/ground reflections. The CCM has the same path loss level as the MCMs in $d_1/d_o < 0.4$. When d_1/d_o is larger than 0.4 the path loss level for both MCMs goes up to 177 dB while that for the CCM decreases to around 155 dB, the free space path loss. This can be explained by referring to Fig. 6a where it can be seen that the LOS region for CCM is when $d_1/d_o \geq 0.7$ but both MCMs are in NLOS for all d_1/d_o ratios. At an elevation angle of 120°, Fig. 9 shows that the CCM and MCM1 have the same path loss in $d_1/d_o < 0.3$. Again, by referring to Figs. 6a and 6b, one can see that both models are in the LOS region. For $d_1/d_o \geq 0.73$ the path loss of MCM1 is less than that for CCM due to the fact that the first order diffraction from B_3 can reach the receiver for MCM1 while no such diffraction exists for CCM.

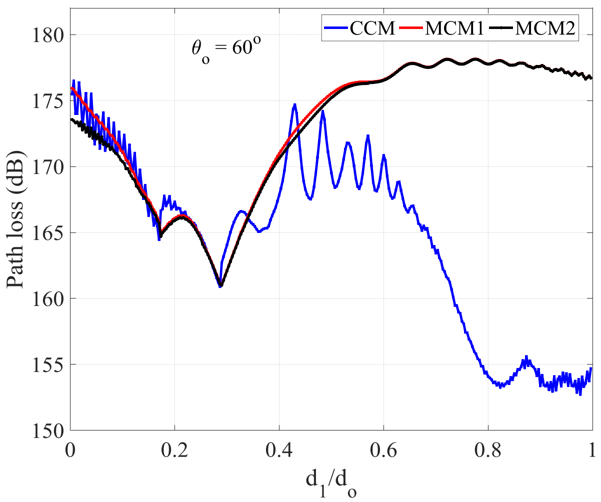

FIGURE 8. Comparison of the wide-band path loss versus d_1/d_o between CCM, MCM1 and MCM2 at $\theta_0 = 60°$ in vertical polarization.

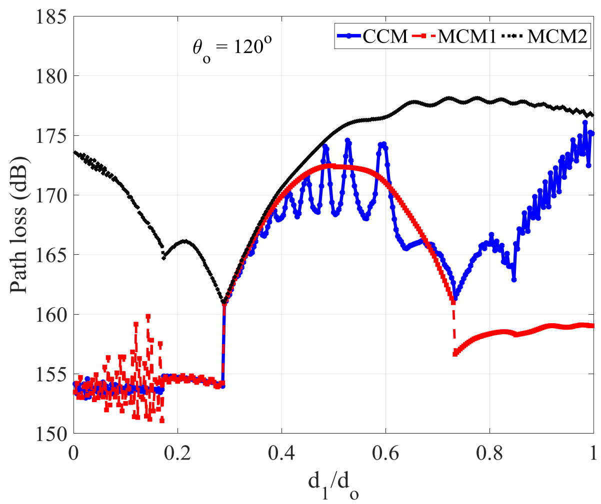

FIGURE 9. Comparison of the wide-band relationship of path loss vs d_1/d_o between CCM, MCM1 and MCM2, at $\theta_0 = 120°$ in vertical polarization.

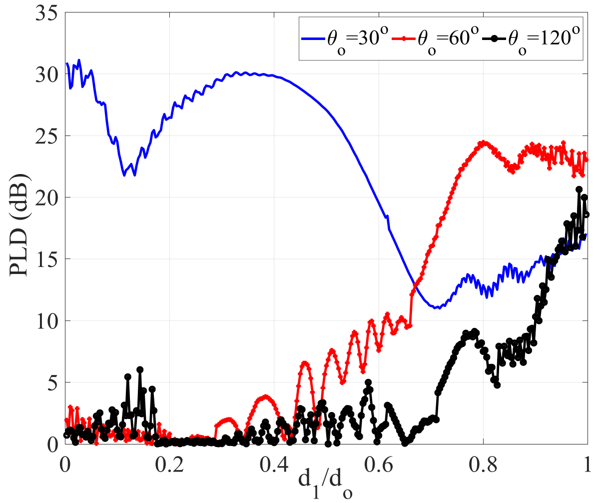

FIGURE 10. Path loss difference (PLD) level between CCM and MCM1.

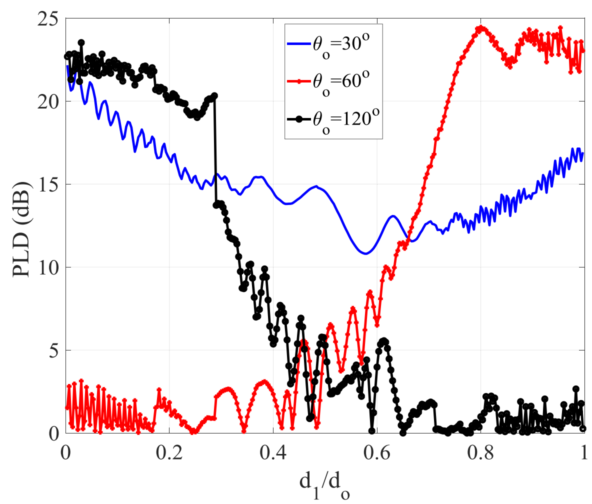

FIGURE 11. Path loss difference (PLD) level between CCM and MCM2.

C. PATH LOSS DIFFERENCE

As already mentioned, the CCM is not accurate in most cases, especially for areas with high-rise buildings such as the one shown in Fig. 1. The path loss difference (PLD) between CCM and both MCMs is calculated as:

$$PLD = L_{CCM} - L_{MCM}(dB) \qquad (16)$$

where L_{CCM} and L_{MCM} are the path loss levels at receiver in CCM and both MCMs using the normalized distance from a building of reference. Figs. 10 and 11 show the path loss difference (PLD) versus d1/do for satellite elevation angles of $\theta_o = 30°$, $60°$ and $120°$. The geometrical parameters are the same as Table 2. Fig. 10 demonstrates the PLD level between CCM and MCM1. As shown in Fig. 10, the maximum PLD level is at the elevation angle of 30°. In this angle the PLD level is between 11dB and 30dB. At $\theta_o = 60^\circ$, in $d_1/d_o < 0.7$ as it can be illustrated in Figs. 6a and 6b, the receiver in CCM and MCM1 is in NLOS1 region. Therefore there is not that much PLD level (less than about 12dB). In $d_1/d_o > 0.7$ receiver in CCM arrives to LOS area, whereas in MCM1 it is still in NLOS1. Thus the PLD level reaches to range of 12 to 25dB. At $\theta_o = 120^\circ$, the minimum PLD level is expected. The reason is that both CCM and MCM1 are in LOS region according to Figs. 6a and 6b. The observed PLD level in the graph is due to diffraction/reflection ray contributions of B_3 demonstrated in Table 1 in MCM1. Fig. 11 shows the PLD level versus d_1/d_o for MCM2. At $\theta_o = 30^\circ$ PLD level due to CCM and MCM2 varies between 12 and 21dB. At $\theta_o = 60^\circ$ the PLD is almost the same as MCM1. It was expected because of the same path loss level at elevation angle of 60° according to Fig. 8. At $\theta_o = 120^\circ$, maximum PLD level is the lower than that of Fig. 10. At this angle, refer to Figs 6.a, and 6.c, in $d_1/d_o < 0.3$, the receiver is in LOS region for CCM whereas it is in NLOS2 region for MCM2.

Therefore, maximum PLD level in $d_1/d_o < 0.3$ is expected. In $d_1/d_o > 0.3$, according to Figs. 6.a and 6.c, the receiver in both CCM and MCM2 arrives in NLOS2 region, as a result the PLD level is reduced drastically.

Table 3 shows the average and the maximum path loss difference between CCM and MCMs for satellite elevation angles from 0° to 180° when receiver is located between buildings B_1 and B_2. The geometrical parameters are the same as Table 2. The path loss difference found in the CCM model shows the importance of MCMs.

TABLE 3. Average and maximum path loss difference between CCM and MCMs when receiver is located between B_1 and B_2.

Propagation Models	Average path loss difference(dB)	Maximum path loss difference (dB)
MCM1	7	22.61
MCM2	11.5	26.38

IV. CONCLUSION

New propagation models for simulating LEO satellite signals in complex urban environments have been introduced. The proposed models are modified versions of the conventional urban canyon model that can take into account the presence of multiple buildings with varying heights. The added buildings lead to varying shadow boundaries and modify the LOS and NLOS regions significantly. Using RT and UTD, multiple realistic scenarios have been simulated and compared to the conventional model. It has been found that the conventional canyon model can severely under-estimate the path loss, by as much as 40 dB, and predict satellite visibility when in reality there is blockage. The proposed modified propagation models could be incorporated into a GNSS simulators/receivers to improve the accuracy of navigation in urban environments.

REFERENCES

[1] J. Marais, D.-F. Nahimana, N. Viandier, and E. Duflos, "GNSS accuracy enhancement based on pseudo range error estimation in an urban propagation environment," *Expert Syst. Appl.*, vol. 40, pp. 5956–5964, Nov. 2013.

[2] M. Vázquez-Castro, F. Pérez-Fontán, and B. Arbesser-Rastburg, "Channel modeling for satellite and HAPS system design," *Wireless Commun. Mobile Comput.*, vol. 2, no. 3, pp. 285–300, 2002.

[3] S. Liu, Z. Niu, and Y. Wu, "A blockage based channel model for high altitude platform communications," in *Proc. 57th IEEE Semiannual Veh. Technol. Conf. (VTC-Spring)*, Apr. 2003, pp. 1051–1055.

[4] J. Holis and P. Pechac, "Elevation dependent shadowing model for mobile communications via high altitude platforms in built-up areas," *IEEE Trans. Antennas Propag.*, vol. 56, no. 4, pp. 1078–1084, Apr. 2008.

[5] J. Holis and P. Pechac, "Penetration loss measurement and modeling for HAP mobile systems in urban environment," *EURASIP J. Wireless Commun. Netw.*, vol. 2008, pp. 1–7, Jan. 2008.

[6] S. K. Agrawal and P. Garg, "Effect of urban-site and vegetation on channel capacity in higher altitude platform communication system," *IET Microw., Antennas Propag.*, vol. 3, no. 4, pp. 703–713, Jun. 2009.

[7] A. Kurniawan, "Propagation loss estimation for urban high altitude platform communications channel," in *Proc. 6th Int. Conf. Telecommun. Syst., Services, Appl. (TSSA)*, Oct. 2011, pp. 246–252.

[8] Z. Hasirci and I. H. Cavdar, "Propagation modeling dependent on frequency and distance for mobile communications via high altitude platforms (HAPs)," in *Proc. 35th Int. Conf. Telecommun. Signal Process. (TSP)*, Jul. 2012, pp. 287–291.

[9] E. T. Michailidis and A. G. Kanatas, "Statistical simulation modeling of 3-D HAP-MIMO channels," *Wireless Pers. Commun.*, vol. 65, pp. 833–841, Aug. 2012.

[10] W. Zhang, "A wide-band propagation model based on UTD for cellular mobile radio communications," *IEEE Trans. Antennas Propag.*, vol. 45, no. 11, pp. 1669–1678, Nov. 1997.

[11] L. J. Luebbers, W. A. Foose, and G. Reyner, "Comparison of GTD propagation model wide-band path loss simulation with measurements," *IEEE Trans. Antennas Propag.*, vol. 37, no. 4, pp. 499–505, Apr. 1989.

[12] P. A. Tirkas, C. M. Wangsvick, and C. A. Balanis, "Propagation model for building blockage in satellite mobile communication systems," *IEEE Trans. Antennas Propag.*, vol. 46, no. 7, pp. 991–997, Jul. 1998.

[13] Z. Blazevic, I. Zanchi, and I. Marinovic, "Deterministic wideband modeling of satellite propagation channel with buildings blockage," *IEEE Trans. Veh. Technol.*, vol. 54, no. 4, pp. 1225–1234, Jul. 2005.

[14] P. S. Mededović and D. S. Šuka, "Softwares for urban electromagnetic wave propagation modeling," *Infoteh-Jahorina*, vol. 11, pp. 422–427, Mar. 2012.

[15] D. R. Iglesias and M. G. Sánchez, "Wideband channel characterization for low-elevation satellites in L-band," *IEEE Trans. Antennas Propag.*, vol. 61, no. 4, pp. 2231–2240, Apr. 2013.

[16] E. Lemos Cid, M. Garcia Sanchez, and A. Alejos, "Wideband analysis of the satellite communication channel at ku- and X-bands," *IEEE Trans. Veh. Technol.*, vol. 65, no. 4, pp. 2787–2790, Apr. 2016.

[17] J. Marais, S. Lefebvre, and M. Berbineau, "Satellite propagation path model along a railway track for GNSS applications," in *Proc. IEEE 60th Veh. Technol. Conf. (VTC-Fall)*, vol. 6, Sep. 2004, pp. 4066–4070.

[18] T. P. K. Nguyen, J. Beugin, and J. Marais, "RAMS analysis of GNSS based localisation system for the train control application," in *Proc. Int. Conf. Comput., Manage. Telecommun. (ComManTel)*, Apr. 2014, pp. 101–106.

[19] A. Bourdeau, M. Sahmoudi, and J. Tourneret, "Tight integration of GNSS and a 3D city model for robust positioning in urban canyons," in *Proc. ION GNSS*, 2012, pp. 1263–1269.

[20] J. Zeleny, P. Pechac, and F. Perez-Fontan, "Generalized propagation channel model for 2 GHz low elevation links using a ray-tracing method," *Radioengineering*, vol. 24, no. 4, pp. 1–6, 2015.

[21] X. Li, R. Vauzelle, Y. Pousset, and P. Combeau, "Hybrid propagation channel modelling for city area land mobile satellite communications," *EURASIP J. Wireless Commun. Netw.*, vol. 2012, pp. 1–13, Dec. 2012.

[22] T. Jost, W. Wang, U.-C. Fiebig, and F. Pérez-Fontán, "A wideband satellite-to-indoor channel model for navigation applications," *IEEE Trans. Antennas Propag.*, vol. 62, no. 10, pp. 5307–5320, Oct. 2014.

[23] A. Abele *et al.*, "A new physical-statistical model of the land mobile satellite propagation channel," in *Proc. 4th Eur. Conf. Antennas Propag. (EuCAP)*, Apr. 2010, pp. 1–5.

[24] M. Z. H. Bhuiyan, J. Zhang, E. S. Lohan, W. Wang, and S. Sand, "Analysis of multipath mitigation techniques with land mobile satellite channel model," *Radioengineering*, vol. 21, pp. 1067–1077, Dec. 2012.

[25] M. Ait-Ighil *et al.*, "Simplifying the propagation environment representation for LMS channel modelling," *EURASIP J. Wireless Commun. Netw.*, vol. 2012, pp. 1–20, Dec. 2012.

[26] M. Ait-Ighil *et al.*, "A three components model for simplified building scattering in urban environment," in *Proc. 6th Eur. Conf. Antennas Propag. (EUCAP)*, Mar. 2012, pp. 2449–2453.

[27] T. Rautiainen, G. Wolfle, and R. Hoppe, "Verifying path loss and delay spread predictions of a 3D ray tracing propagation model in urban environment," in *Proc. IEEE 56th Veh. Technol. Conf. (VTC-Fall)*, Sep. 2002, pp. 2470–2474.

[28] R. Wahl, G. Wölfle, P. Wertz, P. Wildbolz, and F. Landstorfer, "Dominant path prediction model for urban scenarios," in *Proc. 14th IST Mobile Wireless Commun. Summit*, Dresden, Germany, 2005, pp. 1–5.

[29] Y. Seyedi, M. Shirazi, A. Moharrer, S. M. Safavi, and H. Amindavar, "Use of shadowing moments to statistically model mobile satellite channels in urban environments," *IEEE Trans. Wireless Commun.*, vol. 12, no. 8, pp. 3760–3769, Aug. 2013.

[30] K.-W. Kim and S.-J. Oh, "Geometric optics-based propagation prediction model in urban street canyon environments," *IEEE Antennas Wireless Propag. Lett.*, vol. 15, pp. 1128–1131, Oct. 2016.

[31] J. S. Lu, H. L. Bertoni, K. A. Remley, W. F. Young, and J. Ladbury, "Site-specific models of the received power for radio communication in urban street canyons," *IEEE Trans. Antennas Propag.*, vol. 62, no. 4, pp. 2192–2200, Apr. 2014.

[32] A. Jarndal, M. S. A. Salameh, A. Alsaqaf, and Y. Hulba, ''Wideband modeling of land-mobile-satellite channel in built-up environment,'' *J. Electromagn. Anal. Appl.*, vol. 4, no. 3, p. 101, 2012.
[33] R. Paknys, *Applied Frequency-Domain Electromagnetics*. Hoboken, NJ, USA: Wiley, 2016.
[34] R. J. Luebbers, ''A heuristic UTD slope diffraction coefficient for rough lossy wedges,'' *IEEE Trans. Antennas Propag.*, vol. 37, no. 2, pp. 206–211, Feb. 1989.
[35] M. F. Cétedra and J. Perez, *Cell Planning for Wireless Communications*. Norwood, MA, USA: Artech House, 1999.

HOSSEIN HADIDIAN MOGHADAM received the degree in electrical engineer from Islamic Azad University, in 2003, and the M.S. degree in electrical engineering from the Iran University of Science and Technology, in 2006. He is currently pursuing the Ph.D. degree with the École de technologie supérieure, Montreal, Canada. He has been a Research Engineer with the Satellite Communication Group, Iran Telecommunication Research Center. His research interests include propagation and antenna applications for satellite systems, and passive microwave and mm-wave devices.

AMMAR B. KOUKI (S'88–M'92–SM'01) received the B.S. (Hons.) and M.S. degrees in engineering science from Pennsylvania State University, in 1985 and 1987, respectively, and the Ph.D. degree in electrical engineering from the University of Illinois at Urbana–Champaign, in 1991. He is currently a Full Professor of electrical engineering and the Founding Director of the LTCC@ETS Laboratory, École de technologie supérieure, Montreal, Canada. His research interests include active and passive microwave and mm-wave devices and circuits, intelligent and efficient RF front ends, 3-D circuits in LTCC, applied computational electromagnetics, and antennas radio-wave propagation mode.